CdS Nanoparticles Induce a Morphological Transformation of Poly(styrene-*b*-4-vinylpyridine) from Hexagonally Packed Cylinders to a Lamellar Structure

Siao-Wei Yeh and Kung-Hwa Wei*

Department of Materials Science and Engineering, National Chiao Tung University, Hsinchu, Taiwan 30049, ROC

Ya-Sen Sun, U-Ser Jeng, and Keng S. Liang

National Synchrotron Radiation Research Center, 101 Hsin-Ann Road, Science-Based Industrial Park, Hsinchu, Taiwan 30077, ROC

Received November 14, 2004; Revised Manuscript Received March 17, 2005

ABSTRACT: Mercaptoacetic acid-modified CdS nanoparticles disperse selectively in the poly(4-vinylpyridine) domains of poly(styrene-*b*-4-vinylpyridine) (S4VP) block copolymer as a result of the formation of hydrogen bonds. This process in turn induces the morphological transformation of S4VP from a hexagonally packed cylinder structure into a lamellar structure, as evidenced from transmission electron microscopy, atomic force microscopy, and small-angle X-ray scattering studies. This transformation is consistent with that suggested by a theoretical prediction of the phase diagram of the mixed diblock copolymer/nanoparticle system.

Introduction

Block copolymers are versatile platform materials because they self-assemble, under the appropriate compositions and conditions, into various nanostructures that have period thicknesses between 10 and 100 nm as a result of microphase separation between incompatible blocks.[1−10] Several reports have described[11−22] how self-assembled block copolymers in their bulk and thin-film forms can, therefore, be used as templates for incorporating nanoparticles into ordered nanostructures: for example, the segregation of gold nanoparticles into a polystyrene-*b*-poly(ethylene/propylene) block copolymer.[15] Other metal nanoparticles have been formed by in-situ reduction in the microdomain of a block copolymer.[16] Moreover, ordered Au clusters,[17] Co and Fe arrays,[18] and self-assembled Au and Fe_2O_3 nanoparticles[19] have been obtained using micellar solutions of poly(styrene-*b*-4-vinylpyridine) (S4VP). Au, Ag,[20] and magnetic Co[21] nanowires can also be produced by using a PS-*b*-PMMA block copolymer template. The morphologies of block copolymers incorporating nanoparticles can be predicted, as evidenced by a theoretical study presented by the Balazs group.[24] In addition, for semiconductor nanoparticles, selective sequestration has been demonstrated for presynthesized surface-modified CdS and TiO_2 nanoparticles into one block of poly(styrene-*b*-ethylene oxide) (SEO)[25a] and poly(styrene-*b*-methyl methacrylate) (SMMA),[25c] respectively. The morphological transformation of bulk CdS/SEO has also been observed for a high-molecular-weight SEO (PS/PEO = 125K/16.1K; volume fraction of PEO = 0.11). The binding of nanoparticles exclusively to the PEO chains results in a CdS/PEO composite microdomain that has greatly enhanced thermal stability.[25b] Moreover, the sequestered CdS clusters in the PEO domains of SEO block copolymer thin films (PS/PEO = 19K/12.6K; volume fraction of PEO = 0.3) induce a morphological transformation of the PEO microdomain from cylinders to spheres as a result of the formation of hydrogen bonds.[25d]

In this article, we report a morphological transformation of S4VP from a hexagonally packed cylinder structure to a lamellar structure that occurs upon sequestering CdS nanoparticles in the P4VP block. The binding of CdS nanoparticles into the P4VP domains is caused by the formation of hydrogen bonds between them, as evidenced by ^{1}H nuclear magnetic resonance (NMR) spectra and is supported by measurements of glass transition temperatures. Moreover, this morphological transformation induced by CdS nanoparticles is consistent with the phase diagram predicted by a theoretical study of the mixed copolymer/particle system.

Methods

Cadmium acetate dehydrate [$Cd(OAc)_2 \cdot 2H_2O$], sodium sulfide ($Na_2S \cdot 9H_2O$), and mercaptoacetic acid ($HSCH_2COOH$) were purchased from Aldrich. Poly(styrene-*b*-4-vinylpyridine) (S4VP) diblock copolymer having a molecular weight of 47.6KPS/20.9KP4VP (volume fraction of P4VP domains: 0.30) was purchased from Polymersource Inc. [^{1}H NMR ($CDCl_3$): δ = 6.50 (m, H_a), 7.05 (s, H_b), 8.30 (s, H_c)]. CdS nanoparticles (diameter ∼ 3.5 nm) were synthesized by reacting $Cd(OAc)_2 \cdot 2H_2O$ and $Na_2S \cdot 9H_2O$ in methanol in the presence of mercaptoacetic acid as the surfactant, following a modification of the kinetic trapping method.[26] The detailed synthetic procedure has been reported elsewhere.[25] The surfactant makes each CdS nanoparticle hydrophilic by presenting chemically active carboxylic acid groups on the CdS surface, such that the nanoparticles could be dispersed in *N*,*N*-dimethylformamide (DMF). The CdS/DMF dispersion was then added to a previously prepared S4VP/DMF solution under stirring. This mixture was dried slowly under vacuum at 323 K and then maintained at 413 K for 24 h to give the CdS/S4VP nanocomposites. Thermal gravimetric analysis ensured that no residual DMF remained. Using this procedure, we prepared two samples having different nanoparticle content: 7 and 28% CdS (weight fraction with respect to P4VP block).

* To whom correspondence should be addressed: Tel 886-35-731871; Fax 886-35-724727; e-mail khwei@cc.nctu.edu.tw.

10.1021/ma047653a CCC: $30.25
Published on Web 06/28/2005

SAXS measurements were performed at the BL01B beamline of the National Synchrotron Radiation Research Center (NSRRC). The incident beam, extracted from a superconducting-wavelength-shifter (SWLS) X-ray source, was monochromated to a wavelength λ of 1.55 Å by a Ge (111) double-crystal monochromator, with $\Delta\lambda/\lambda \sim 10^{-3}$. The 0.5 mm diameter beam used was mainly collimated by one set of slits followed by two sets of pinholes in ~5 m. With a sample-to-detector distance of 1571 mm, we collected SAXS data using a 50 mm linear detector of 80 μm pixel resolution. With the highly collimated beam and fine spatial resolution of the detector, the data in the Q range measured were with a $(\Delta Q/Q)$ resolution less than 5%, where the wave vector transfer Q $(= 4\pi \sin(\theta/2)/\lambda)$ was defined by the scattering angle θ and λ of X-rays. All the SAXS data were corrected for sample transmission, background, and the detector sensitivity, and the Q value was calibrated by a commonly used silver behenate. The detailed SAXS setup and instrument calibration were reported recently.[31] Transmission electron microscopy was performed on a Hitachi H-600 instrument operating at 100 kV and on a JEOL-2010 TEM operating at 200 kV at the Center for Nano Science & Technology (CNST). The ultrathin sections of CdS/S4VP nanocomposites prepared for TEM studies were microtomed using a Leica Ultracut Uct apparatus equipped with a diamond knife and subsequently deposited on copper grids. The microtomed thin films, corresponding to the section of the CdS/S4VP nanocomposites, were also observed using a Digital Nanoscope IIIa atomic force microscope (AFM). For studies of hydrogen bonding, ^{1}H NMR spectra were recorded on a Varian Unity 300 MHz NMR spectrometer using d_8-toluene as the solvent. The glass transition temperatures (T_g) of the samples were obtained using a Dupont DSC 2910 instrument at a heating rate of 10 °C/min.

Results and Discussion

Figure 1 displays TEM (left-hand side) and phase contrast AFM (right-hand side) images of the S4VP samples containing different amount of CdS nanoparticles. From the phase-contrast AFM images, we provide the surface morphology about PS and P4VP domains of the microtomed samples, and the distributions of the heavy atom, iodine or cadmium, in the microtomed samples with 50−80 nm thickness are shown by the projected transmission images TEM. In the TEM image of S4VP (Figure 1a), the dark region, obtained by staining with iodine, is the P4VP domain and the light region is the PS domain. In this image, the round- and cylindrical-shaped dark regions represent cross-sectional and side views, respectively, of the cylindrical P4VP domains. The pure S4VP has a hexagonally packed cylindrical (HEX) structure that is constituted by 23 nm diameter P4VP cylinders that have an intercylinder distance of 52 nm. This cylindrical morphology is also displayed in the phase-contrast AFM image of the microtomed S4VP thin films: the light-colored round and linear areas represent cross sections and oblique cross sections of the cylindrical P4VP phases; the dark regions represent the PS domains. As shown in Figure 1b,c, the AFM images are matched with the TEM images, which suggests CdS nanoparticles are located in P4VP domains and there is no substantial tilt in the TEM images. However, the phase contrast of AFM images does not change upon particle sequestration. In the presence of 7% CdS nanoparticles, as indicated in Figures 1b, the dark-colored zones in the TEM image represent the P4VP/CdS composite phase; they appear dark because of the higher electron density of cadmium atoms. The CdS nanoparticles in this case are segregated selectively in the P4VP domains, apparently through the mediation of dipole−dipole interactions between the carboxylic acid groups of mercaptoacetic acid on the CdS surface and the P4VP chains. The CdS/S4VP sample, however, has transformed into a lamellar structure that consists of alternating 28 nm thick PS and 12 nm thick CdS/P4VP lamellae. The volume ratio of the CdS/P4VP domains in the lamellar CdS/S4VP composite is ca. 0.3, as determined by the lamellae thicknesses; this value matches that calculated by the molecular weight. In Figure 1b, small dark CdS aggregates (darker spots), however, seem to be observed in P4VP lamellae. The aggregation behavior of CdS in the P4VP region of block copolymer can also be determined from higher magnification TEM image on these spots in the P4VP lamellae. The inserted higher magnification TEM image shows that CdS nanoparticles remain in the P4VP lamellae loosely, not densely, indicating CdS nanoparticles are in a nonaggregated state. Nevertheless, the CdS-rich domains (darker spots in the CdS/P4VP lamellae), containing also well-dispersed CdS nanoparticles, may precipitate out from the ordered lamellar domains of CdS/P4VP and form a third stable phase (or some kinetically trapped intermediate state) in the system, when the CdS concentration is above a critical concentration (which is, apparently, smaller than 7%). From the TEM images, the CdS-rich P4VP domains start to precipitate out in 7% CdS/S4VP and expand widely in the 28% CdS sample. In the 28% CdS/S4VP sample, the growth of CdS-rich P4VP already intervene significantly with the lamellar structure and deteriorate substantially the long-range order except that the local lamellar structure still remains, as indicated by the TEM and AFM images presented in Figure 1c.

In addition, we examined the morphologies of the pure S4VP block copolymers and the S4VP samples containing segregated CdS nanoparticles by one-dimensional small-angle X-ray scattering (SAXS). Figure 2a displays SAXS curves of pure S4VP and CdS/S4VP obtained using synchrotron radiation. For pure S4VP, structure factor peaks appear at $Q = 0.0137$, 0.0234, 0.0357, and 0.0408 Å^{-1}, which correspond to a ratio of $1:3^{1/2}:7^{1/2}:9^{1/2}$. This ratio is consistent with the typical scattering expected for a structure containing hexagonally packed cylinders (HEX). Using eq 1, we determined the intercylinder distance (D) to be 53 nm:

$$D = (3/2)^{1/2} d_{100} \tag{1}$$

where $d_{110} = 2\pi/Q_{110}$ and $Q_{110} = 0.137$ nm^{-1}.

In the case of S4VP containing 7% CdS in the P4VP domains, the scattering peaks are located at $Q = 0.0137$, 0.0273, and 0.0404 Å^{-1}, corresponding to a ratio of 1:2:3, which implies that the scattering is caused by a lamellar structure. The SAXS results, being consistent with the TEM results, also suggest strongly that the HEX structure of pure S4VP transformed into a lamellar morphology in the presence of CdS nanoparticles. Figure 2b,c shows the detailed analysis for the SAXS data of the samples containing 7% and 28% CdS in the CdS/P4VP domains. In the analysis, we decompose the scattering intensity into $I(Q) = P(Q)S(Q)$, where the form factor, $P(Q)$, stands for the scattering contribution from the shape of the scattering objects and the structure factor, $S(Q)$, for the interference effect between the objects. In our previous report, we have shown that $P(Q)$ for the copolymer/nanoparticle composite is contributed by the scattering from the CdS nanoparticles and the copolymer blocks. Using spheres of a mean radius of

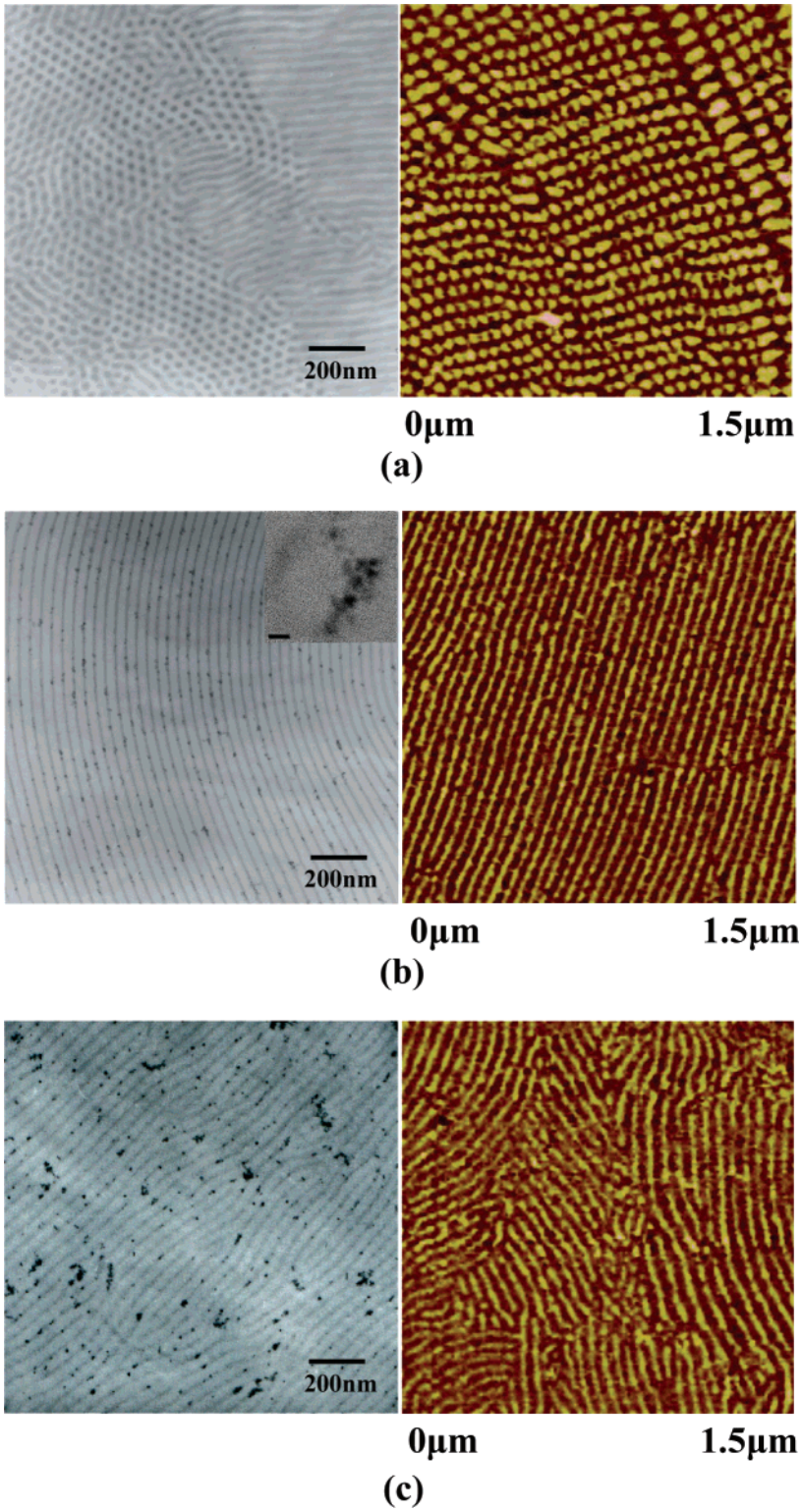

Figure 1. Transmission electron microscopy (left-hand side) and phase contrast atomic force microscopy (right-hand side) images of bulk pure S4VP and S4VP samples containing 7 and 28 wt % CdS particles. The scale bar of the inserted TEM image in the 7% CdS/S4VP is 10 nm.

17.5 Å and a polydispersity of 50% for the form factor of CdS nanoparticles $P_1(Q)$, we can fit the data in the higher Q region (dashed curve), as derived in our previous report for the CdS nanoparticles.[25b] On the other hand, the form factor contribution of the P4VP slabs, $P_2(Q)$, can be approximated by the Kratky−Porod approximation with $P_2(Q) \sim \exp(-Q^2t^2/12)$, where t is the slab thickness. This approximation should be adequate in the Q ranged measured, on the basis of the long slabs observed in TEM and AFM images.[30] Using the approximation of $P(Q) \sim P_1(Q) + P_2(Q)$ derived in our previous study for the nanoparticle−copolymer composite,[25b] we can fit (solid curve) most of the SAXS data well with a P4VP slab thickness of 11.2 nm, for the 7% CdS/S4VP sample. The structure factor extracted from $S(Q) = I(Q)/P(Q)$ for the composite (circles) is fitted (short dashed curve) using three Lorentzian profiles with peaks located at 0.014, 0.0273, and 0.0404

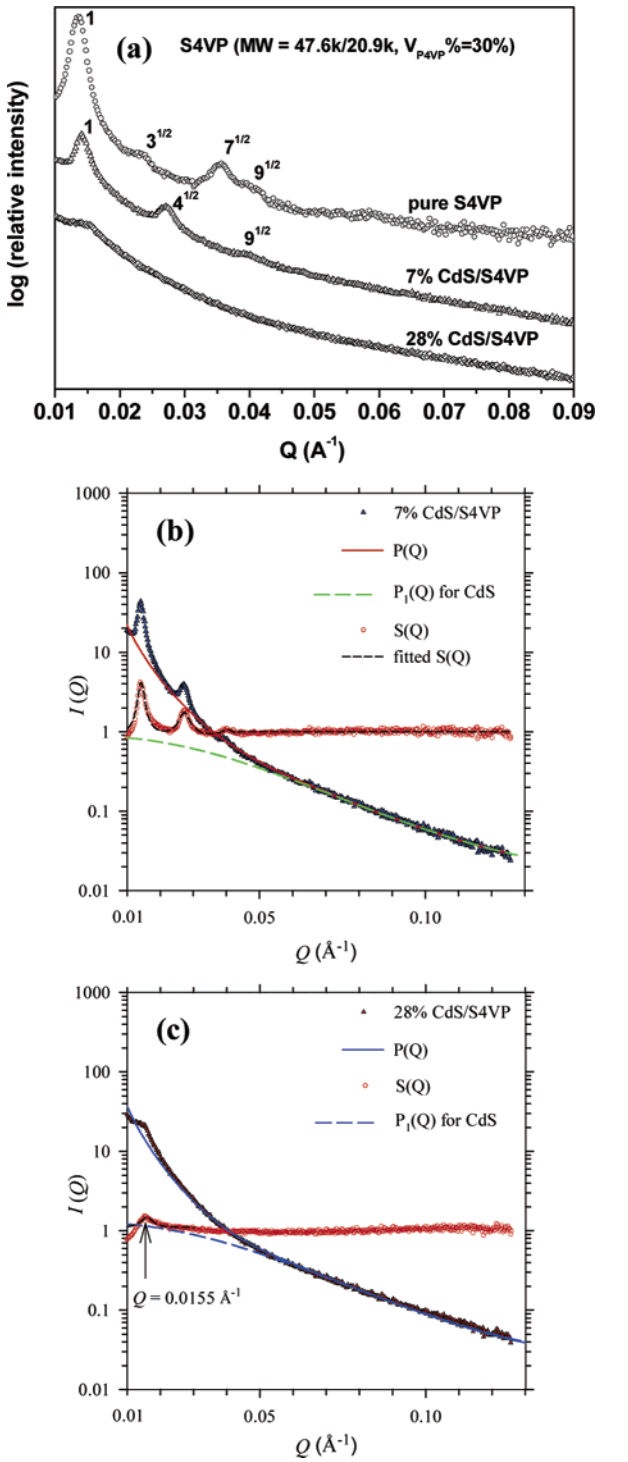

Figure 2. (a) Small-angle X-ray scattering curves of pure S4VP and S4VP samples containing 7 and 28% CdS nanoparticles. (b) SAXS data (triangles) for 7% CdS/S4VP. The form factor $P(Q)$ (solid curve) of the composite is a summation of the scattering contributions of the CdS nanoparticles (long dashed curve) and the P4VP slabs. The extracted structure factor $S(Q)$ (circles) is fitted (short dashed curve) using three Lorentzian profiles of peaks located at 0.014, 0.0273, and 0.0404 Å^{-1}, respectively. These peaks together suggest a lamellar spacing of 43.9 nm. Note that the first peak position is slightly affected by the Kratky−Porod approximation used, as discussed previously. (c) SAXS data (triangles) for 28% CdS/S4VP. The form factor $P(Q)$ (solid curve) of the composite is a summation of the scattering contributions of the CdS nanoparticles (long dashed curve) and the P4VP slabs. The extracted structure factor of the composite (circles) is fitted with a Lorentzian profile (short dashed curve) of a peak at Q = 0.0155 Å^{-1}.

Å^{-1}. The periodic Q interval 0.0137 Å^{-1} corresponds to a lamellar spacing of 45.9 nm for Bragg scattering. The thickness for the P4VP/CdS layers and the lamellar spacing for the system obtained from SAXS match closely with the TEM and AFM measurements.

On the other hand, for the sample of 28% CdS/S4VP, we can fit most of the SAXS data (solid curve in Figure 2c) with a form factor consisting of the contributions from CdS nanoparticles of the same structural characteristics as the previous case and the P4VP slabs of a mean slab thickness of 12.4 nm. Using the $P(Q)$ obtained, we deduce $S(Q)$ from $I(Q)/P(Q)$, which exhibits only one clear interference peak for the sample (circles in Figure 2c). We fit the $S(Q)$ using a Lorentzian profile. From the scattering peak, Q = 0.0155 Å^{-1}, and peak width fitted, we deduce a lamellar spacing of ∼40.5 nm and a lamellar domain size of ∼0.3 μm (corresponding to ∼7−8 periodic layers). These results are roughly consistent with the TEM and AFM images. It should be noted that a contraction of the lamellar spacing with increasing CdS content as shown in the SAXS data in Figure 2a (first reflection of 28% sample shifts to higher q as compared to the 7% sample), which is contrary to the TEM and AFM results. The discrepancy (dilation vs contraction) between the imaging analysis and the SAXS results of the lamellar spacing upon the CdS filling content might be explained by the following two factors. First, the TEM and AFM images display only local images in the composite sample, which could not represent the dilation of the lamellar spacing accurately. Second, the lamellar spacing 40.5 nm obtained from the SAXS result is about ∼10% smaller than that observed from the TEM and AFM images. Likely, the lamellar spacing determined from SAXS using the only one interference peak with the Bragg condition may not be accurate enough for a quantitative comparison. As can be seen from the TEM and AFM images, the lamellar ordering of the sample of 28% CdS is significantly deteriorated, and it resulted in a larger polydispersity in the lamellar spacing. Thus, the interference peak in the SAXS profile observed may not reflect the lamellar spacing through the simple Bragg law. To extract accurately the lamellar spacing of the system, we may need to take the polydispersity effect in the lamellar spacing into account. Additionally, the form factor contribution can also affect the interference peak position, as shown in the revised SAXS analysis. In our previous report,[25e] a similar shift of SAXS results was also shown in the CdS/PS-*b*-PEO system while the cylindrical ordering looses.

Regarding the particle distribution in the CdS/block copolymer system, the SAXS profiles for both samples of 7% and 28% CdS do not show the typical Q^{-4} power law scattering of large aggregates in the low Q region. The result indicates that the CdS nanoparticles inside the CdS/P4VP domains, including the CdS-rich CdS/P4VP domains, of the two samples are well dispersed in the block copolymer. This result is consistent with our previous rigorously observation for the CdS nanoparticles in solutions as well as in copolymer composites.[25b] Scheme 1 illustrates the morphological transformations and the destruction of long-range ordering for the S4VP block copolymers at the various CdS contents and represents the changes of the characteristic distribution of CdS, based on the TEM and SAXS results.

Scheme 1. Hydrogen Bonding Induces the Morphological Transformation from the HEX Structure of Pure S4VP Block Copolymers to Lamellar CdS/S4VP Composites upon Selective Segregation of CdS Nanoparticles into the P4VP Phase[a]

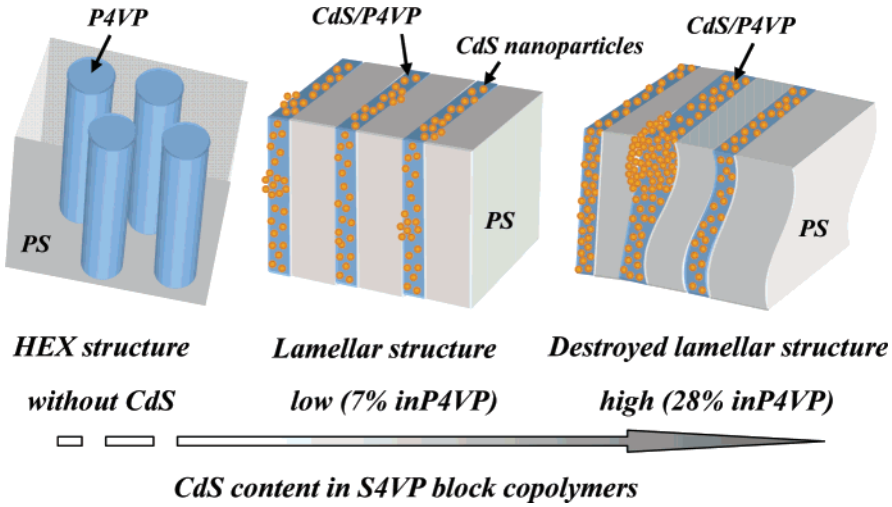

[a] Overloading of CdS nanoparticles in the P4VP domains causes curvature of the CdS/P4VP lamellar domains and structural destruction as a result of CdS aggregation.

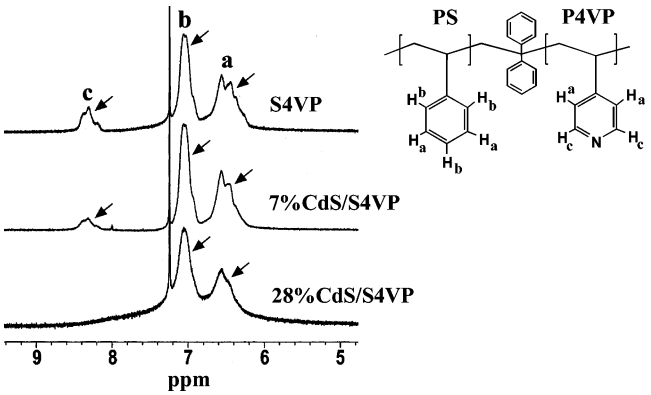

Figure 3. ^{1}H NMR spectra of pure S4VP and S4VP samples containing 7 and 28% CdS nanoparticles (weight fraction with respect to the P4VP block).

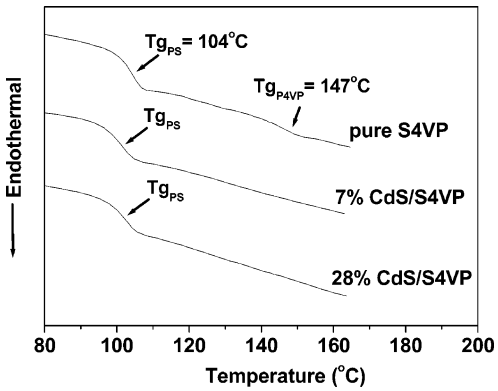

Figure 4. DSC thermograms displaying the glass transition temperatures of the PS and P4VP domains of pure S4VP and S4VP samples containing 7 and 28% CdS nanoparticles.

We note that the amounts of CdS nanoparticles, 7 and 28 wt % with respect to the P4VP block, are ca. 2.7 and 10.8% by effective particle volume fraction that taken into account the ligand shell; the values are not sufficient to swell the P4VP phases into regions of a lamellar structure having volume fractions between 0.4 and 0.6. The morphological transformation from the cylindrical pure S4VP to lamellar CdS/S4VP can be mediated by strong interaction forces, such as hydrogen bonds, between the carboxylic acid units of the CdS nanoparticles and the poly(4-vinylpyridine) chains. Figure 3 displays partial ^{1}H NMR spectra of pure S4VP and CdS/S4VP containing 7 and 28% CdS in P4VP. In these spectra, peak **b** at 7.05 ppm corresponds to the protons of the phenyl rings in the PS block ($\mathbf{H_b}$); they are unaffected by the presence of CdS nanoparticles in P4VP domains. The relative intensity of peaks **c** (8.30 ppm) and **a** (6.50 ppm), however, decreases upon increasing the amount of CdS nanoparticles. Peak **c** represents protons in the pyridine rings ($\mathbf{H_c}$), whereas peak **a** reflects protons in both the pyridyl and phenyl rings ($\mathbf{H_a}$). In the presence of the CdS nanoparticles, the ratio of peaks **c** and **b** reduced from 0.23 for pure S4VP to 0.12 for 7% CdS/S4VP. Peak **c** disappeared in the spectrum of 28% CdS/S4VP. The ratio of peaks **a** and **b** reduced from 0.95 for pure S4VP to 0.85 for 7% CdS/S4VP and to 0.68 for 28% CdS/S4VP. The reduction in the peak intensity of the signals of the hydrogen atoms $\mathbf{H_a}$ and $\mathbf{H_c}$ in the pyridine rings indicates the loss of mobility in these pyridine rings as a result of the formation of hydrogen bonds between the carboxylic acid groups on the surface of the CdS nanoparticles and the P4VP chains; similar conclusions have been presented in an earlier report.[27,29]

Further evidence of the loss of mobility of the P4VP chains that occurs upon binding of the CdS nanoparticles appears from an analysis of the glass transition temperatures of the P4VP chains ($T_{g,P4VP}$). Figure 4 displays the DSC thermograms of pure S4VP and the CdS/S4VP samples containing 7 and 28% CdS in P4VP. In pure S4VP, the glass transitions of the PS ($T_{g,PS}$) and P4VP ($T_{g,P4VP}$) chains appear clearly at 104 and 147 °C, respectively. In the presence of 7 and 28% CdS in P4VP, however, only $T_{g,PS}$ is observed, which indicates that the mobility of the P4VP chains is retarded by the presence of the CdS nanoparticles.

A theoretical study on diblock copolymer/nanoparticle composites was reported recently by the Balazs group, who generated phase diagrams to predict the structural transitions of mixed A−B block copolymer/particle systems upon variations in the particle interactions.[24c] Assuming that the P4VP blocks are unper-

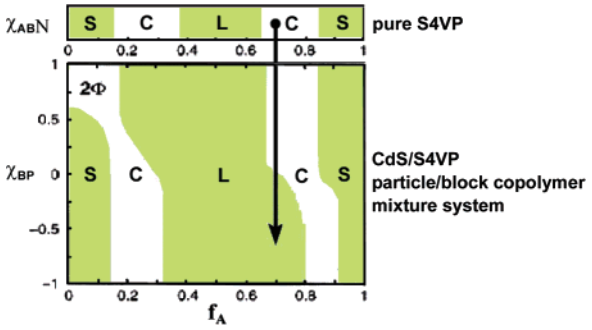

Figure 5. Phase diagram of the morphological transformation from the HEX structure of pure S4VP block copolymers to the lamellar structure upon selective segregation of CdS nanoparticles in the P4VP phase. This diagram is a modification of Figure 1a of ref 24c.

turbed Gaussian chains, we estimated the radius of gyration of the P4VP chains to be 45.9 Å by using the expression $R_g = (1/6)^{1/2}aN^{1/2}$, where a is the statistical segment length ($a_{P4VP} = 7.97$ Å)[28] and N is the degree of polymerization ($N_{P4VP} = 199$). With regard to the phase diagram presented in Figure 5, which we have modified from ref 24c, A, B, P, and χ correspond to PS, P4VP, CdS, and the enthalpic interaction in our system, respectively, and f_A refers to the fraction of PS segments in a S4VP chain ($f_A = 0.7$ in this case). The S4VP diblock copolymer was under the strong segregation limit ($\chi_{AB}N > 100$).[24c,29,30] The size of CdS particle (R_p = ca. 18.4 Å) can be described as $R \approx 0.4R_g$. In the pure S4VP system, as shown in Figure 5, the morphology is determined only by the volume fraction; an HEX morphology is obtained. In the presence of 7% CdS, however, the value of χ_{BP} is negative as a result of the presence of hydrogen bonds between the P4VP domains and the CdS nanoparticles. In the phase diagram of the block copolymer/particle mixture system, the negative value of χ_{BP} causes the morphological transformation from a cylindrical to a lamellar structure, which is consistent with our experimental results. As CdS content is increased up to 28%, the deformation of the lamellar structure and the loss of long-range order can be explained by the fact that the large numbers of CdS nanoparticles fill up the large fraction of free space in the P4VP domains, which segregate irregularly. Balazs et al. have suggested that self-assembled structures could be either stable or metastable, depending on the volume faction and particle size.[24a]

Conclusions

CdS nanoparticles that segregate into the P4VP domains of S4VP block copolymers, in a process mediated by the formation of hydrogen bonds, induce the morphological change of the CdS/S4VP composites from hexagonally packed P4VP cylinders to a lamellar structure. The experimental data we have obtained for the morphological transformation of these CdS/S4VP composites are consistent with theoretical predictions of the stability of such nanoparticle/block copolymer systems.

Acknowledgment. The authors thank the National Science Council and the US Air Force Office of Scientific Research for funding this work through Grants NSC 92-2120-M-009-001 and AOARD-03-4018, respectively.

References and Notes

(1) (a) Bates, F. S.; Fredrickson, G. H. *Annu. Rev. Phys. Chem.* **1990**, *41*, 525. (b) Bates, F. S. *Science* **1991**, *251*, 898.
(2) (a) Reiter, G.; Castelein, G.; Sommer, J.-U.; Rollele, A.; Thurn-Albrecht, T. *Phys. Rev. Lett.* **2001**, *87*, 226101. (b) Rottele, A.; Thurn-Albrecht, T.; Sommer, J. U.; Reiter, G. *Macromolecules* **2003**, *36*, 1257.
(3) Li, L.; Serero, Y.; Koch, M. H. J.; de Jeu, W. H. *Macromolecules* **2003**, *36*, 529.
(4) Jiang, S.; Gopfert, A.; Abetz, B. *Macromolecules* **2003**, *36*, 6171.
(5) (a) Zhu, L.; Huang, P.; Chen, W. Y.; Weng, X.; Cheng, S. Z. D.; Ge, Q.; Quirk, R. P.; Senador, T.; Shaw, M. T.; Thomas, E. L.; Lotz, B.; Hsiao, B. S.; Yeh, F.; Liu, L. *Macromolecules* **2003**, *36*, 3180. (b) Zhu, L.; Cheng, S. Z. D.; Huang, P.; Ge, Q.; Quirk, R. P.; Thomas, E. L.; Lotz, B.; Hsiao, B. S.; Yeh, F.; Liu, L. *Adv. Mater.* **2002**, *14*, 31.
(6) (a) Segalman, R. A.; Hexemer, A.; Kramer, E. J. *Macromolecules* **2003**, *36*, 6831. (b) Segalman, R. A.; Hexemer, A.; Kramer, E. J. *Phys. Rev. Lett.* **2003**, *91*, 196101.
(7) (a) Choi, S.; Lee, K. M.; Han, C. D.; Sota, N.; Hashimoto, T. *Macromolecules* **2003**, *36*, 793. (b) Chen, H. L.; Hsiao, S. C.; Lin, T. L.; Yamauchi, K.; Hasegawa, H.; Hashimoto, T. *Macromolecules* **2001**, *34*, 671.
(8) (a) Buck, E.; Fuhrmann, J. *Macromolecules* **2001**, *34*, 2172. (b) Nick, L.; Lippitz, A.; Unger, W.; Kindermann, A.; Fuhrmann, J. *Langmuir* **1995**, *11*, 1912.
(9) Sundrani, D.; Darling, S. B.; Sibener, S. J. *Nano Lett.* **2004**, *4*, 273.
(10) (a) Knoll, A.; Horvat, A.; Lyakhova, K. S.; Krausch, G.; Sevink, G. J. A.; Zvelindovsky, A. V.; Magerle, R. *Phys. Rev. Lett.* **2002**, *89*, 35501. (b) Rehse, N.; Knoll, A.; Magerle, R.; Krausch, G. *Macromolecules* **2003**, *36*, 3261.
(11) (a) Forster, S.; Antonietti, M. *Adv. Mater.* **1998**, *10*, 195. (b) Chernyshov, D. M.; Bronstein, L. M.; Borner, H.; Berton, B.; Antonietti, M. *Chem. Mater.* **2000**, *12*, 114.
(12) Lazzari, M.; Lopez-Quintela, M. A. *Adv. Mater.* **2003**, *19*, 1583.
(13) Park, C.; Yoon, J.; Thomas, E. L. *Polymer* **2003**, *44*, 6725.
(14) Hamley, I. W. *Nanotechnology* **2003**, *14*, R39.
(15) (a) Bockstaller, M. R.; Lapentnikov, Y.; Margel, S.; Thomas, E. L. *J. Am. Chem. Soc.* **2003**, *125*, 5276. (b) Bockstaller, M.; Kolb, R.; Thomas, E. L. *Adv. Mater.* **2001**, *13*, 1783.
(16) (a) Ribbe, A. E.; Okumura, A.; Matsushige, K.; Hashimoto, T. *Macromolecules* **2001**, *34*, 8239. (b) Hashimoto, T.; Harada, M.; Sakamoto, N. *Macromolecules* **1999**, *32*, 6867.
(17) (a) Haupt, M.; Miller, S.; Glass, R.; Arnold, M.; Sauer, R.; Thonke, K.; Moller, M.; Spatz, J. P. *Adv. Mater.* **2003**, *15*, 829. (b) Spatz, J. P.; Herzog, T.; Mobmer, S.; Ziemann, P.; Moller, M. *Adv. Mater.* **1999**, *11*, 149.
(18) (a) Abes, J. I.; Cohen, R. E.; Ross, C. A. *Chem. Mater.* **2003**, *12*, 1125. (b) Boontongkong, Y.; Cohen, R. E. *Macromolecules* **2002**, *35*, 3647.
(19) Sohn, B. H.; Choi, J. M.; Yoo, S.; Yun, S. H.; Zin, W. C.; Jung, J. C.; Kanehara, M.; Hirata, T.; Teranishi, T. *J. Am. Chem. Soc.* **2003**, *125*, 6368.
(20) (a) Lopes, W. A.; Jaeger, H. M. *Nature (London)* **2001**, *414*, 735. (b) Lopes, W. A. *Phys. Rev. E* **2002**, *65*, 031606.
(21) Bal, M.; Ursache, A.; Tuominen, M.; Goldbach, J. T.; Russell, T. P. *Appl. Phys. Lett.* **2002**, *81*, 3479.
(22) (a) Cheng, J. Y.; Ross, C. A.; Chan, V. Z.-H.; Thomas, E. L.; Lammertink, R. G. H.; Vancso, G. J. *Adv. Mater.* **2001**, *13*, 1174. (b) Cheng, J. Y.; Ross, C. A.; Thomas, E. L.; Smith, H. I.; Vancso, G. J. *Adv. Mater.* **2003**, *15*, 1599.
(23) Fogg, D. E.; Radzilowski, L. H.; Blanski, R.; Schrock, R. R.; Thomas, E. L. *Macromolecules* **1997**, *30*, 417.
(24) (a) Huh, J.; Ginzburg, V. V.; Balazs, A. C. *Macromolecules* **2000**, *33*, 8085. (b) Thompson, R. B.; Ginzburg, V. V.; Matsen, M. W.; Balazs, A. C. *Science* **2001**, *292*, 2469. (c) Lee, J. Y.; Thompson, R. B.; Jasnow, D.; Balazs, A. C. *Macromolecules* **2002**, *35*, 4855.
(25) (a) Yeh, S. W.; Wei, K. H.; Sun, Y. S.; Jeng, U. S.; Liang, K. S. *Macromolecules* **2003**, *36*, 7903. (b) Jeng, U. S.; Sun, Y. S.; Lee, H. Y.; Hsu, C. H.; Liang, K. S.; Yeh, S. W.; Wei, K. H. *Macromolecules* **2004**, *37*, 4617. (c) Weng, C. C.; Wei, K. H. *Chem. Mater.* **2003**, *15*, 2936. (d) Yeh, S. W.; Chang, Y. T.; Chou, C. H.; Wei, K. H. *Macromol. Rapid Commun.* **2004**, *25*, 1679. (e) Yeh, S. W.; Wu, T. L.; Wei, K. H.; Sun, Y. S.; Liang, K. S. *J. Polym. Sci., Part B: Polym. Phys.* **2005**, *43*, 1220.
(26) (a) Veinot, J. G. C.; Ginzburg, M.; Pietro, W. J. *Chem. Mater.* **1997**, *9*, 2117. (b) Herron, N.; Wang, Y.; Eckert, H. *J. Am. Chem. Soc.* **1990**, *112*, 1322.

(27) (a) Chen, D.; Peng, H.; Jiang, M. *Macromolecules* **2003**, *36*, 2576. (b) Peng, H.; Chen, D.; Jiang, M. *J. Phys. Chem. B* **2003**, *107*, 12461. (c) Yao, X.; Chen, D.; Jiang, M. *J. Phys. Chem. B* **2004**, *108*, 5225.

(28) Bolline, C.; Stone, V. W.; Carlier, V.; Jonas, A. M. *Macromolecules* **1999**, *32*, 4718.

(29) (a) Ruokolainen, J.; Makinen, R.; Torkkeli, M.; Serimaa, R.; ten Brink, G.; Ikkala, O. *Science* **1998**, *280*, 557. (b) Polushkin, E.; Albertda van Ekenstrin, G. O. R.; Knaapila, M.; Ruokolainen, J.; Torkkeli, M.; Serimaa, R.; Bras, W.; Dolbnya, I.; Ikkala, O.; ten Brink, G. *Macromolecules* **2001**, *34*, 4917. (c) Clarke, C. J.; Eisenberg, A.; Nguyen, D.; Schwarz, S. A.; Strzhemechny, Y.; Sauer, B. B. *Macromolecules* **1997**, *30*, 4184.

(30) Porod, G. In *Small Angle X-ray Scattering*; Glatter, O., Kratky, O., Eds.; Academic Press: London, 1980; p 17.

(31) Lai, Y. H.; Sun, Y. S.; Jeng, U. S.; Huang, Y.-S.; Song, Y. F.; Tsang, K. L.; Liang, K. S. *Nucl. Instrum. Methods Phys. Res. B*, in press.

MA047653A